



## MATERIALS SCIENCE

# Glass transition temperature as a unified parameter to design self-healable elastomers

Jae-Man Park<sup>1†</sup>, Chang Seo Park<sup>1†</sup>, Sang Kyu Kwak<sup>2</sup>, Jeong-Yun Sun<sup>1,3\*</sup>

Self-healing ability of materials, particularly polymers, improves their functional stabilities and lifespan. To date, the designs for self-healable polymers have relied on specific intermolecular interactions or chemistries. We report a design methodology for self-healable polymers based on glass transition. Statistical copolymer series of two monomers with different glass transition temperatures ( $T_g$ ) were synthesized, and their self-healing tendency depends on the  $T_g$  of the copolymers and the constituents. Self-healing occurs more efficiently when the difference in  $T_g$  between two monomer units is larger, within a narrow  $T_g$  range of the copolymers, irrespective of their functional groups. The self-healable copolymers are elastomeric and nonpolar. The strategy to graft glass transition onto self-healing would expand the scope of polymer design.

Copyright © 2024 the Authors, some rights reserved; exclusive licensee American Association for the Advancement of Science. No claim to original U.S. Government Works. Distributed under a Creative Commons Attribution NonCommercial License 4.0 (CC BY-NC).

## INTRODUCTION

Self-healing materials are of great advantages for preserving their original functionality and extending their lifespan (1, 2). Viscoelastic nature of polymers, wherein the polymer networks can restore elastic energy or flow under external load, potentiates their self-healing from mechanical damage (3, 4). The potential has led to intensive studies on developing self-healable polymers over decades (5).

To achieve self-healing, polymer chains require sufficient mobility and interchain interactions (Fig. 1A) (5). Therefore, many studies have investigated to incorporate diverse molecular interactions, including hydrogen bonding (6–12), host-guest chemistry (13, 14), metal-ligand coordinations (15–18), ionic (19–22), hydrophobic (23), ion-dipole (24, 25),  $\pi$ - $\pi$  (26, 27), van der Waals (28), and dipole-dipole interactions (29, 30), into flexible polymer networks or gels (plasticized networks). Dynamic covalent bonds (31–33) or hard-soft multiphase (34, 35) has also been incorporated into the polymer networks for self-healing.

Since the interchain interactions and the chain mobility were considered individual properties, the paradigm of designing self-healable polymers has been focused on finding specific chemistries or molecular interactions and applying them to flexible chains. We believed and hypothesized that a simple but holistic parameter would exist in designing self-healable polymers. In this work, we present a design methodology for self-healable polymers based on glass transition (Fig. 1B). We synthesized a series of statistical (random) copolymers of two nonpolar acrylic monomer units with different  $T_g$  values (Fig. 1C). We found that the self-healing tendency can be explained by the  $T_g$  values of both the copolymers and the constituent monomer units.

## RESULTS

When polymer chains have a  $T_g$  lower than room temperature (RT), the chains can flow because of enough chain mobility, whereas when polymer chains have a  $T_g$  higher than RT, the chains are rigid because

of interchain interactions, such as molecular interactions or frictions. We thought that tailoring the  $T_g$  of polymers and their constituent segments would be a methodological approach to designing self-healable polymers (Fig. 1B). To verify our conception, we designed random copolymers composed of two types of commercial nonpolar acrylate monomers as a model system (Fig. 1C). One monomer segment has a  $T_g$  higher than RT, while the other segment has a  $T_g$  lower than RT. The former segment with diverse functional groups is referred to as  $R_H$ , whereas the latter as  $R_L$ . A series of copolymer films with diverse  $R_H$ - $R_L$  combinations were prepared by bulk free-radical polymerization. Briefly, the two kinds of monomers were mixed with varying their compositions, and then 0.1 wt % of a photoinitiator was added. The precursor solutions were cured by ultraviolet (UV) light for 12 hours with a film shape. The obtained films were cut into desired shapes for further tests (see Materials and Methods for details). The synthesized copolymers have relatively high molecular weights (table S1).

We conducted tensile stress-stretch tests for the copolymer series at RT (figs. S1 to S9). To evaluate the self-healing ability of the copolymers, we cut the middle region of the copolymer films, reattached the two damaged surfaces within a minute, healed the samples for 24 hours at RT in air, and conducted the same tensile tests. Self-healing efficiency  $\eta_{\text{heal}}$  was defined as the strain energy density ratio of healed to pristine samples (Fig. 2A). For  $R_H$  = phenyl (Ph) and  $R_L$  = *n*-butyl (Bu) copolymer series (Ph-Bu), as the molar ratio of  $R_H$  ( $\chi_h$ ) increases, the stiffness increases and the stretchability decreases consistently (fig. S1) while the  $\eta_{\text{heal}}$  of the copolymer series peaks at medium  $\chi_h$  value (Fig. 2B). Similar mechanical and self-healing tendency are observed in different  $R_H$ -Bu series, such as *tert*-butyl (tBu) (fig. S3), cyclohexyl (Chx) (fig. S4), and isobornyl (Isb) (fig. S5). However, for benzyl (Bz)-Bu series, where the  $R_H$  segment has similar functional group with Ph (aromatic), as  $\chi_h$  increases, a similar mechanical tendency is observed (fig. S2), but self-healing is inefficient (Fig. 2D). For 2-hydroxyethyl (He)-Bu series, where the  $R_H$  segment has polar functional group (weak hydrogen bonding), self-healing is also inefficient (Fig. 2E and fig. S6).

The difference in self-healing behavior between the peak-having copolymer series and the less healable series would be originated from the  $T_g$  value of  $R_H$  segments, rather than from specific molecular interactions. Despite having same aromatic functional group, Ph-based ( $T_g$  = 47°C) and Bz-based ( $T_g$  = 6°C) copolymer series exhibit distinct

<sup>1</sup>Department of Materials Science and Engineering, Seoul National University, Seoul 08826, Republic of Korea. <sup>2</sup>Department of Chemical and Biological Engineering, Korea University, Seoul 02841, Republic of Korea. <sup>3</sup>Research Institute of Advanced Materials (RIAM), Seoul National University, Seoul 08826, Republic of Korea.

\*Corresponding author. Email: jysun@snu.ac.kr

†These authors contributed equally to this work.

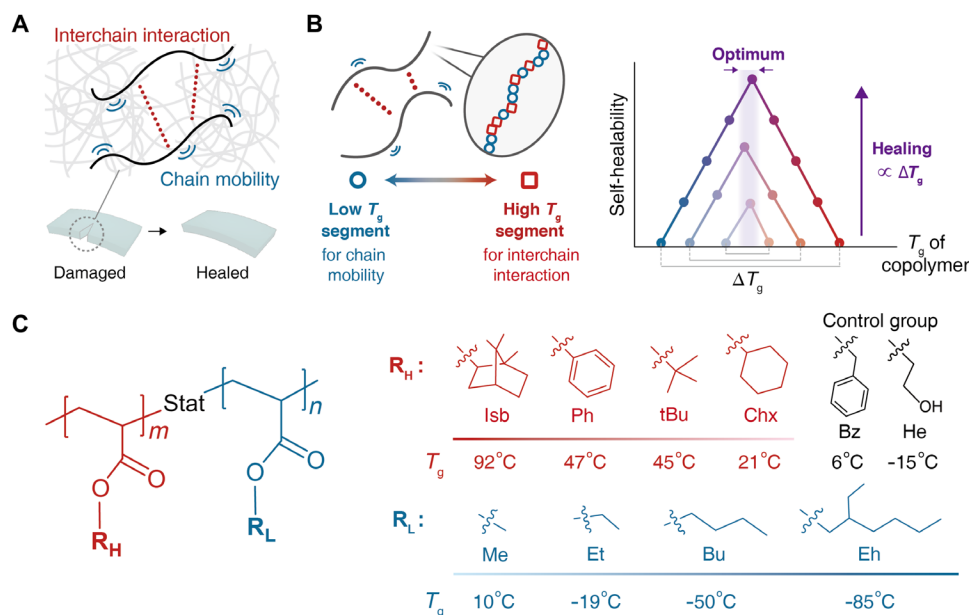


**Fig. 1. The design methodology for self-healable polymers based on glass transition.** (A) Self-healing of polymers occurs by two factors: interchain interaction and chain mobility. (B) The two factors can be regulated by glass transition temperature ( $T_g$ ) of copolymers and their constituents. (C) Statistical copolymers with two types of acrylate monomer units, where one has high  $T_g$  that stores the interaction energy (named  $R_H$ ), and the other has low  $T_g$  that gives the mobility to polymer chains (named  $R_L$ ). Diverse  $R_H$  and  $R_L$  with nonpolar hydrocarbon functional groups are introduced to investigate the self-healing of copolymers. Bz and He are control functional groups for the investigation of molecular interaction effects on the self-healing phenomenon.

self-healing behaviors, with the difference in  $\eta_{\text{heal}}$  more than 60%. Even the weak hydrogen bonding of He ( $T_g = -15^\circ\text{C}$ ) copolymer series does not assure their self-healing. Instead, when the  $R_H$  segment has a  $T_g$  higher than RT, the copolymer series show high  $\eta_{\text{heal}}$  at an optimum  $\chi_h$ .

The  $T_g$ -dependent self-healing behavior is more evident when the  $R_H$  segment is fixed to tBu, and the  $R_L$  segment is varied from methyl (Me;  $T_g = 10^\circ\text{C}$ ) to ethyl (Et;  $T_g = -19^\circ\text{C}$ ), Bu ( $T_g = -50^\circ\text{C}$ ), and 2-ethylhexyl (Eh;  $T_g = -85^\circ\text{C}$ ) (Fig. 2C and figs. S3 and S7 to S9). Each copolymer series has optimum self-healing compositions, where the peak  $\eta_{\text{heal}}$  value gradually increases, shifts to higher  $\chi_h$ , and narrows as the  $T_g$  of  $R_L$  segment decreases. For the case of tBu-Eh series when  $\chi_h$  is 0.8 (named tBu-Eh-0.8),  $\eta_{\text{heal}}$  reaches over 100%, indicating that the polymer completely recovers its mechanical properties (Fig. 2A). The fracture of healed copolymer samples occurs at the positions similar to those of pristine samples, which suggests complete self-healing (fig. S10). The mechanical damage at the cut interfaces starts to recover immediately after contact (fig. S11). Self-healing of Isb-Eh and Ph-Eh series is also investigated (figs. S12 and S13).

The self-healing tendency of copolymer series is affected by the  $T_g$  of constituting monomer segments, which raised the question of whether the  $T_g$  of copolymer itself would be related to self-healing. We measured the  $T_g$  of copolymer series (Fig. 2F and figs. S14 and S15). The  $T_g$  of copolymer series is linearly proportional to  $\chi_h$  (Fig. 2, G and H, fig. S16, and see Supplementary Text) (36). The self-healable copolymers that show peak  $\eta_{\text{heal}}$  have narrowly distributed  $T_g$  values between  $1^\circ$  and  $16^\circ\text{C}$  (Fig. 2I). The  $T_g$  of copolymers with  $\eta_{\text{heal}}$  more than 60% is more narrowly distributed between  $1^\circ$  and  $9^\circ\text{C}$  (movie S1). From a self-healing perspective, polymer chains

should have both enough interchain interaction and chain mobility. In the designed copolymers, the  $R_H$  segment can store elastic energy facilitated by interchain interactions, whereas the  $R_L$  segment enables polymer chains to be mobile at given temperature. The specific functional groups of each segment can function differently within the copolymers, which leads to the different optimum self-healing composition in various monomer combinations of the copolymers. Nevertheless, the copolymers collectively converge to the optimum thermodynamic state for self-healing at different components and compositions, resulting in the narrowly distributed  $T_g$  of highly self-healable copolymers. This optimum compositional behavior of diverse copolymers for self-healing has been reported in recent studies (28, 29, 37), while we emphasize that the glass transition can explain the optimum self-healing behaviors appeared in diverse copolymer series.

On the other hand, each segment in the polymer chains still plays a role in self-healing. The  $R_H$  segment with higher  $T_g$  would give more interchain interactions, while the  $R_L$  segment with lower  $T_g$  would give more chain mobility to their copolymer chain. From this perspective, we plotted the peak  $\eta_{\text{heal}}$  against the  $T_g$  difference between  $R_H$  and  $R_L$  segments of the copolymer ( $\Delta T_g$ ), and notable distributions can be observed (Fig. 2J). The higher  $\Delta T_g$  leads to more self-healable copolymer series (movie S2). Note that a poly(methyl acrylate) (pMeA) homopolymer, whose  $T_g$  ( $10^\circ\text{C}$ ) locates in the peak self-healing region, does not self-heal efficiently because of the absence of the role of  $R_H$  and  $R_L$  segments (fig. S17).

To understand those  $T_g$ -dependent self-healing tendencies, we plotted the  $\eta_{\text{heal}}$  of tBu-Eh copolymer series as a function of time (Fig. 3, A and B). Self-healing occurs most efficiently at optimum  $\chi_h$  of 0.8, with the fastest approach to completing healing within a day

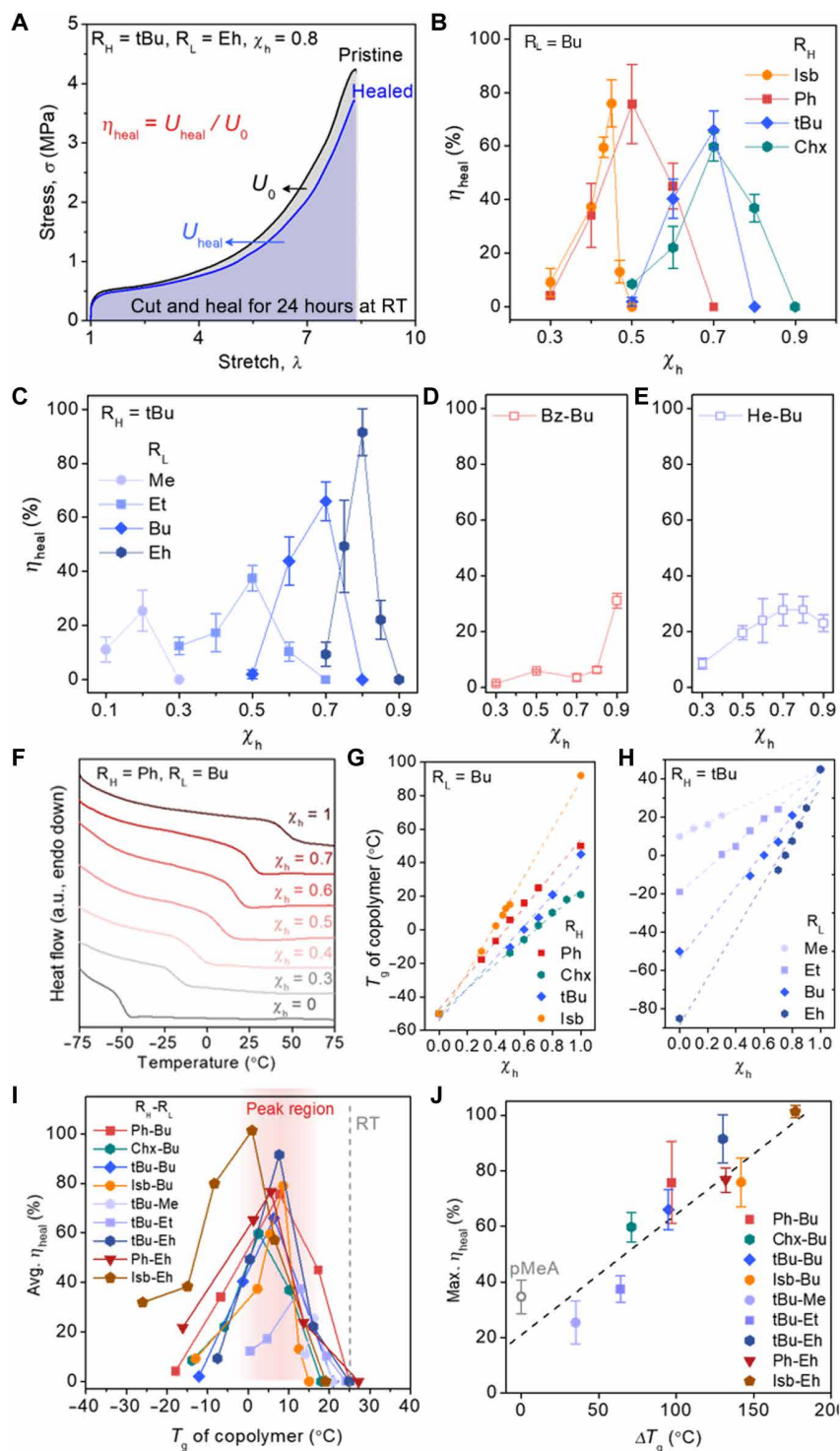


**Fig. 2. Self-healing tendency in the copolymers.** (A) Stress-stretch curves of a pristine and a cut-and-healed copolymer films.  $R_H$ ,  $R_L$ , and  $\chi_h$  of the copolymers are tBu, Eh, and 0.8, respectively. Self-healing efficiency ( $\eta_{heal}$ ) is defined as the strain energy density ratio of healed ( $U_{heal}$ ) to pristine ( $U_0$ ) samples. (B)  $\eta_{heal}$  values of diverse copolymer series as a function of  $\chi_h$ , where  $R_L$  is fixed to Bu and  $R_H$  is Isb, Ph, tBu, and Chx, respectively. (C)  $\eta_{heal}$  values of copolymer series as a function of  $\chi_h$ , where  $R_H$  is fixed to tBu and  $R_L$  is varied from Me to Eh. (D and E)  $\eta_{heal}$  values of control copolymer series as a function of  $\chi_h$ , where  $R_L$  is fixed to Bu and  $R_H$  is low  $T_g$  aromatic Bz (D) and low  $T_g$  polar He group (E), respectively. (F) Differential scanning calorimetry (DSC) curves of the Ph-Bu copolymer series. Zero and 1 of  $\chi_h$  represent the DSC curves of Bu and Ph homopolymer, respectively. a.u., arbitrary units. (G and H)  $T_g$  of copolymer series as a function of  $\chi_h$ . The dashed lines are the linear fits for each copolymer series. (I) Averaged  $\eta_{heal}$  values of diverse copolymer series as a function of  $T_g$ . Peak data of  $\eta_{heal}$  are located in  $T_g$  of  $1^{\circ}$  to  $16^{\circ}C$  (red-colored area). (J) Maximum  $\eta_{heal}$  values of diverse copolymer series as a function of the difference of  $T_g$  between  $R_H$  and  $R_L$  homopolymers ( $\Delta T_g$ ). The dashed line is a guide to the eye. Error bars in (B) to (E) and (J) denote SDs;  $N = 3$ .

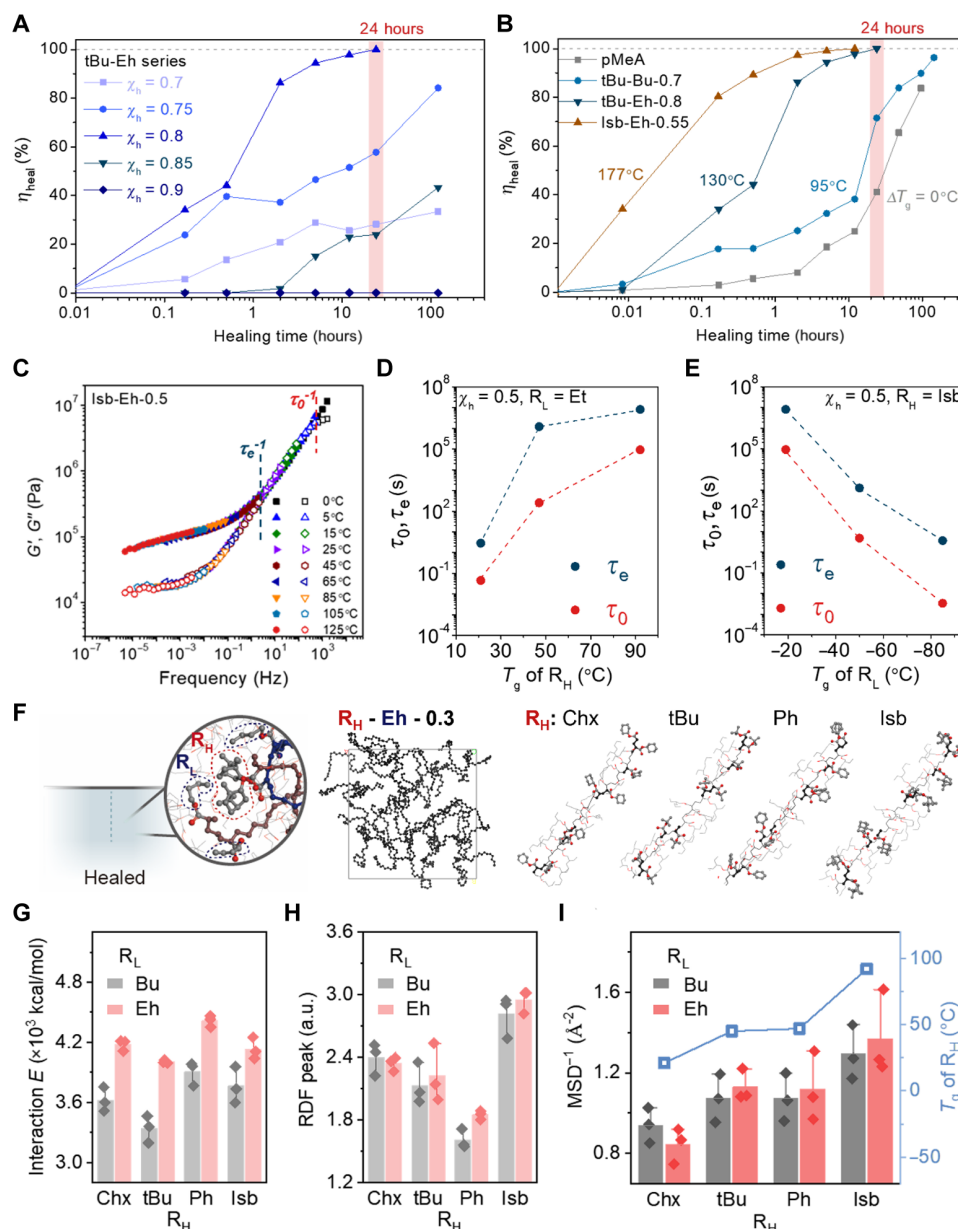


**Fig. 3. Proposed self-healing mechanism.** (A) Time-dependent  $\eta_{\text{heal}}$  values of the copolymers with varying compositions. (B) Time-dependent  $\eta_{\text{heal}}$  values of the copolymers with varying  $\Delta T_g$ . (C) Representative master curves of storage ( $G'$ ) and loss ( $G''$ ) modulus of the copolymer Isb-Eh-0.5 obtained by classical time-temperature superposition. (D and E)  $\tau_0$  and  $\tau_e$  of the copolymer series as a function of the  $T_g$  of  $R_H$  (D) and the  $T_g$  of  $R_L$  (E). The  $\chi_h$  of the copolymer series is fixed to 0.5. (F) Schematic of constituent segments in copolymer and molecular structure of  $R_H$ -Eh-0.3 random copolymers with varying  $R_H$  segments. Black ball and stick model represents the backbone chain of polymers. The tacticity and the location of  $R_H$  segments are same for the copolymers. Bu and Eh were considered as  $R_L$  segments. (G) Calculated interaction energy of copolymers according to the  $R_H$  segment species. (H) The first peak value of radial distribution function (RDF) of  $R_H$ - $R_H$  segments in copolymer series. (I) Inverse of the calculated mean square deviation (MSD) and experimentally determined  $T_g$  of  $R_H$  homopolymer. Error bars in (G) to (I) denote SDs;  $N = 3$ .

(Fig. 3A). Note that when the healing temperature is increased, self-healing is accelerated (fig. S18). For the tBu-Eh-0.7, where the ratio of  $R_H$  segment is insufficient than the optimum composition, self-healing occurs gradually but slow because of insufficient interchain interactions. A slight increase in  $\chi_h$  to 0.75 accelerates self-healing, where the copolymer is expected to heal completely at a certain time, which would be more than 100 hours. When the ratio of  $R_H$  segment is excessive than optimum composition ( $\chi_h$  of 0.85), the

copolymer did not heal within 2 hours and then slowly begins to heal because of inadequate chain mobility. Self-healing did not occur when the  $R_H$  segment is too excessive ( $\chi_h$  of 0.9).

When the  $T_g$  of copolymer series is in the optimum range, all copolymer series tend to heal completely, while self-healing occurs faster when the  $\Delta T_g$  is larger (Fig. 3B). This phenomenon presents an important implication: Since the balance between the interchain interaction and the chain mobility is revealed by the  $T_g$  of copolymers,



the copolymers with optimum  $T_g$  can heal themselves, even for pMeA homopolymer. However, the  $T_g$  of each segment affects the self-healing speed, where the required time to complete healing is more than 20 times for tBu-Bu-0.7 ( $\Delta T_g = 95^\circ\text{C}$ ) compared to Isb-Eh-0.55 ( $\Delta T_g = 177^\circ\text{C}$ ). That is, the role of each segment during the healing process can be elucidated by their homopolymer  $T_g$  themselves.

To investigate the role of each segment in the copolymer series, we conducted rheological experiments (Fig. 3, C to F). Since the copolymers were synthesized without cross-linkers, they can be regarded as linear entangled polymer melts (38). Three types of relaxation time exist in the system: Kuhn segmental relaxation time ( $\tau_o$ ), entanglement relaxation time ( $\tau_e$ ), and bulk relaxation time ( $\tau_b$ ). Those relaxation times can be obtained from the reciprocals of three crossovers in the frequency-dependent rheological responses (fig. S19). The rheological responses of the copolymer series were obtained with classical time-temperature superposition method (Fig. 3C and figs. S20 and S21). When the  $\chi_h$  and  $R_L$  were fixed to 0.5 and Et, respectively, the  $\tau_o$  and the  $\tau_e$  increased by several orders as the  $T_g$  of  $R_H$  increased (Fig. 3D). That means that the  $R_H$  segment restricts the movement of polymer chains, which acts as physical interchain interactions in the networks. The higher  $T_g$  of  $R_H$  segment provides higher interchain interactions in the same composition of  $R_H$  segment. When the  $\chi_h$  and  $R_H$  were fixed to 0.5 and Chx, respectively, the  $\tau_o$  and the  $\tau_e$  decreased by several orders as the  $T_g$  of  $R_L$  decreased (Fig. 3E). Those tendency means that the  $R_L$  segment plasticizes the copolymer chains. The lower  $T_g$  of  $R_L$  segment provides higher chain mobility in the same composition of  $R_L$  segment. In the above experiments, there is no consideration on the molecular structure of functional groups; rather, we only consider the  $T_g$ , which means that the self-healing of nonpolar polymers depends on glass transition. Note that the  $\tau_b$  for all copolymer series is greater than 2700 hours (110 days), which means that the self-healing of the copolymers does not originate from bulk relaxation.

In general, for a polymer to be self-healing, it should have a  $T_g$  lower than healing temperature, but not every polymer with a  $T_g$  below the environmental temperature is capable of self-healing (5). Through our experiments, we presented that the high  $T_g$  segment is crucial for the self-healing. Therefore, the role of  $R_H$  segments on the self-healing of copolymer has been studied in detail using molecular dynamics (MD) simulations (Fig. 3, F to I, figs. S22 to S26, and see Materials and Methods and Supplementary Text for details). We considered a series of  $R_H$ - $R_L$ -0.3 random copolymers with varying  $R_H$  segment species at  $25^\circ\text{C}$  and 1 atm (Fig. 3F). The location of  $R_H$  segments and the tacticity were kept the same for all considered copolymers. The Bu and Eh were considered as  $R_L$  segments. The calculated interaction energy between polymer chains, defined as an interatomic nonbonded interaction of van der Waals and electrostatic interaction, presents that the copolymers with Ph segment exhibit the highest interaction energy due to  $\pi$ - $\pi$  interaction between Ph groups (Fig. 3G). Radial distribution function (RDF) provides structural information that describes the position of the analyzed segments relative to the reference segment. While the RDF values of  $R_L$ - $R_L$  segments of copolymer series remain identically (fig. S23), those values of  $R_H$ - $R_H$  segments were different where the copolymers with Isb segments exhibit the highest peak value at the first shell distance (Fig. 3H and fig. S24), indicating that the structural aggregation is more predominant in the Isb groups. These two interchain interactions, the intermolecular interaction and the

structural aggregation, do not show a dependency with  $T_g$  but mutually influence the dynamics of polymer chains. The movement of the amorphous copolymers is represented by a mean square deviation (MSD). The inverse of calculated MSD of the copolymers, which represents the degree of restriction of chain movement, is consistent with the trend in the  $T_g$  of copolymer, where the higher  $T_g$  presents larger movement restriction in the copolymers (Fig. 3I). This implies that the  $R_H$  segments could function as physical interactions through friction within the polymer network, akin to conventional specific moieties used in designing self-healing polymers.

In the context of self-healing, the interchain interactions in polymers play a crucial role to facilitate self-healing, which can serve as a strong driving force to restore interfacial damages. The healing process of the copolymer follows the established healing mechanism (fig. S26 and see Supplementary Text). In the nonpolar polymer system, the driving force of interchain interaction originates from  $R_H$  segments. In Figs. 2I and 3A, at low  $\chi_h$ , the lack of the interactions delays self-healing, while at high  $\chi_h$ , the excess of the interactions causes the lack of chain mobility, which delays self-healing either. Thus, the optimum always appears at a specific composition, and it is located within the narrow range of  $T_g$  in terms of glass transition.

While in Figs. 2J and 3B, higher  $\eta_{\text{heal}}$  at a certain healing time and faster healing speed are observed with larger  $\Delta T_g$ . The higher  $T_g$  of the  $R_H$  segment corresponds to more effective physical interaction sites in the polymer network, and the lower  $T_g$  of the  $R_L$  segment guarantees the amount of  $R_H$  segment for the optimum  $T_g$ . For example, the self-healing behavior of tBu-Eh-0.8 is faster than that of tBu-Bu-0.7 due to larger  $\chi_h$ , while Isb-Eh-0.55 presents faster self-healing behavior than tBu-Bu-0.7 despite smaller  $\chi_h$  due to stronger interaction effect of Isb group than that of tBu group, as represented by their homopolymer  $T_g$  (Fig. 3I). Since the  $T_g$  of copolymers and their constituents connotes both the effect of interchain interaction and chain mobility simultaneously, we can eventually design self-healing polymers by  $T_g$  as a unified parameter.

Existing self-healable elastomers have often shown yielding at small stretch (24, 25) or large residual stretch and slow recovery (17, 30, 39). For example, poly(*n*-butyl acrylate) has very low  $T_g$  and self-healing properties, while it shows yielding at small stretch (fig. S27). The highly self-healable copolymers exhibit elastic properties (Fig. 4, A and B, and movie S3), including fast recovery with small residual stretch ( $\lambda \sim 1.7$ ) after large applied stretch  $\lambda_{\text{app}} = 7$  (Fig. 4C), as well as low Young's modulus  $E$ , moderate tensile strength  $\sigma$ , and large stretchability  $\lambda$  (fig. S28). The values of  $E$ ,  $\sigma$ , and  $\lambda$  of the self-healable copolymer series were 1 to 3 MPa, 1 to 4 MPa, and 6 to 10, respectively. Among them, the elastic behaviors of the representative self-healable copolymers (tBu-Eh-0.8, Ph-Eh-0.65, and Isb-Eh-0.55) were investigated and compared with commercially available Bu rubber (fig. S29). When the copolymer series were loaded and unloaded, they returned to its original shape with small residual stretch and mechanical hysteresis (Fig. 4C and fig. S29, B and C). At small  $\lambda_{\text{app}}$ , the copolymer series act as damping elastomers with large hysteresis (fig. S29D). While at large stretch ( $\lambda_{\text{app}} > 4$ ), the copolymer series were more elastic than Bu rubber, with smaller hysteresis and residual stretch (fig. S29E). After first loading and unloading of the tBu-Eh-0.8 copolymer, direct reloading showed weaker mechanical strength. However, after 5 min from the unloading, the copolymer recovered its tensile strength completely (Fig. 4D). Tensile stress relaxation curves of the copolymer and Bu rubber showed similar tendency,

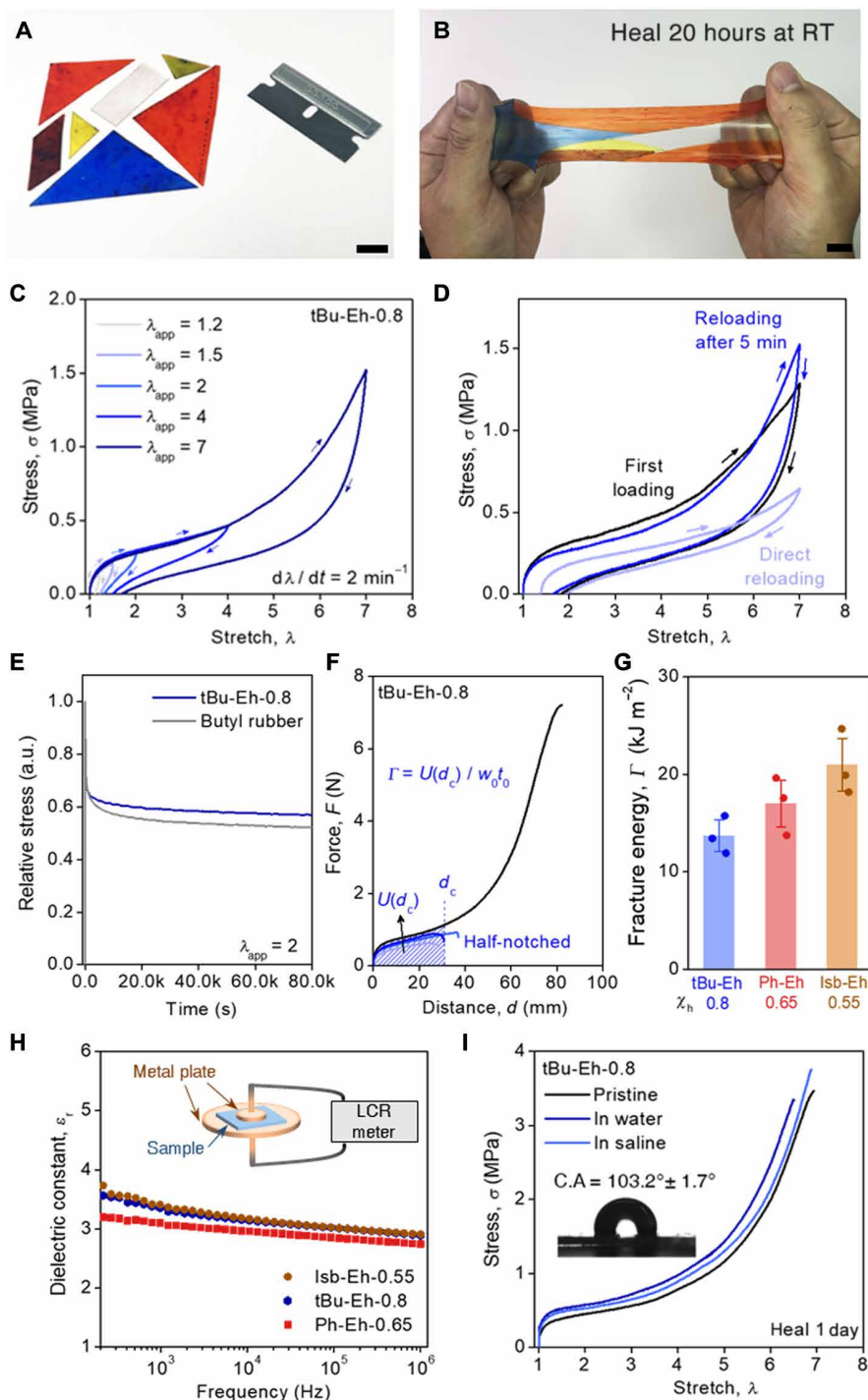


**Fig. 4. The self-healable copolymers are rubbery and nonpolar.** (A and B) Photographs of the cut (A) and reassembled (B) self-healable rubbery copolymers. Scale bars, 1 cm. (C) Tensile loading and unloading hysteresis cycle of the tBu-Eh-0.8 copolymers with varying applied stretch ( $\lambda_{app}$ ). The stretch rate is  $2 \text{ min}^{-1}$ . The copolymer exhibits moderate hysteresis even under large stretches. Although the polymer is stretched up to 7, the residual stretch is only 1.7 after unloading. (D) The copolymers are firstly loaded and unloaded with  $\lambda_{app}$  of 7, and then one sample is reloaded immediately, while the other sample is reloaded after 5 min with the recovery of its strength. (E) Stress relaxation of the copolymer and commercial Bu rubber. The  $\lambda_{app}$  is 2, measured at RT. (F) Force-distance curves of the rubber (tBu-Eh-0.8). The black line is unnotched sample, and the blue-colored lines are half-notched samples. Fracture energy ( $\Gamma$ ) is defined as the work done by unnotched sample until the critical distance of notched sample ( $d_c$ ),  $U(d_c)$ , divided by the width ( $w_0$ ) and the thickness ( $t_0$ ) of unnotched sample. (G) Fracture energy of the representative nonpolar self-healable rubber series. Error bars denote SDs;  $N = 3$ . (H) Dielectric constant  $\epsilon_r$  of the copolymer series as a function of frequency. Inset shows a schematic of the dielectric spectra measurement. (I) Stress-stretch curves of the copolymers healed in aqueous environment. The samples were cut in water or saline (35 per mil of NaCl solution) and then attached and healed in water or saline for 24 hours at RT. Inset shows photograph image of water microdroplet on the tBu-Eh-0.8 copolymer. The average water contact angle (C.A.) is  $103.2^\circ$  with the SD of  $1.7^\circ$ .

where the copolymer preserved relative stress more than Bu rubber for 80,000 s (Fig. 4E and fig. S30). The residual stretch was less than 0.04 after released from applied stretch of  $\lambda_{\text{app}} = 2$  (fig. S31). The fracture energy of the copolymer series is 13 to 25 kJ m<sup>-2</sup> (Fig. 4, F and G, and fig. S32), comparable to that of natural rubbers (40).

The self-healing copolymer series are nonpolar, as expected from their nonpolar parents comprising hydrocarbon functional groups. The dielectric constant  $\epsilon_r$  of the copolymers is from 3 to 3.3 at 1 kHz (Fig. 4H), and the dielectric loss (or loss tangent)  $\epsilon''/\epsilon'$  of them is below 0.1 to 0.02 (fig. S33). The following feature is hydrophobicity, where the copolymer is self-healable under aqueous environment (Fig. 4I). Other features of the copolymers include transparency (fig. S34) and air stability from the absence of volatile or hygroscopic compounds (fig. S35).

## DISCUSSION

The proposed copolymer design has shown a  $T_g$ -dependent self-healing behavior, where it presents as an analogous way to the existing designs for self-healing polymers. Although the microscopic behavior of self-healing in polymers is complicated, we can design the self-healable copolymers by simply regulating a macroscopic property: the glass transition. The nonpolarity of the copolymers reveals the self-healing tendency, where the self-healing does not rely on specific molecular interactions. Further, the attempt to graft glass transition onto self-healing would expand the design scope of polymer science and engineering. The simplicity of the design parameter and synthetic method may be useful for materials engineers to grant self-healability to diverse polymer types with desired features. Potential applications include the design of encapsulation materials for stretchable electronics, dielectric elastomers for actuators and sensors, polymer electrolytes, or commercial rubbers.

## MATERIALS AND METHODS

### Materials

All monomers used in this work were purchased from Sigma-Aldrich and TCI Chemicals. A photoinitiator [2-hydroxy-2-methyl propiophenone (HMPP)] was purchased from TCI Chemicals. All chemicals were used as received.

### Copolymer synthesis

Monomers of desired combinations and compositions were mixed with 0.1 vol % of HMPP photoinitiator. As a typical example, for the copolymer of tBu-Eh-0.8, 2.92 ml of tBu acrylate, 1.04 ml of Eh acrylate, and 4  $\mu$ l of HMPP were mixed using magnetic stirrer. After nitrogen gas bubbling for 5 min, the precursor solution was injected to customized molds, consisting of two Teflon-taped glass slides with 400- $\mu$ m-thick stacked polyethylene terephthalate (PET) film spacer. Then, the polymerization was carried out under 365-nm UV irradiation (CL-1000L, UVP) for 12 hours. After that, the upper glass was removed, and the copolymer film was heated on hot plate at 90°C for 3 hours to remove unreacted monomers. The other copolymer films were fabricated with the same procedure, with varying their combination and composition.

### Molecular weight measurement

The number-average molecular weight  $M_n$ , weight-average molecular weight  $M_w$ , and polydispersity index of the representative copolymer

series were determined by gel permeation chromatography (Young Lin YL9100 high-performance liquid chromatography system) coupled with a refractive index detector (Young Lin YL9170 RI detector) and three columns. Tetrahydrofuran (Samchun Chemicals, high-performance liquid chromatography, stabilized, >99.9%) was used as the eluent at 35°C with a flow rate of 0.7 ml min<sup>-1</sup>. Polymethylmethacrylate standards were used for calibration.

### Mechanical and self-healing tests

For the tensile tests, the fabricated copolymer films were cut into 5 mm by 20 mm by 0.4 mm (width  $\times$  length  $\times$  thickness). The copolymer films were then mounted into the holding grips of a universal testing machine (Instron 3343) with a 50-N load cell. The gauge length of all specimen was fixed to 10 mm. Stretch rate was kept constant at 5 min<sup>-1</sup> unless specified. All mechanical tests were performed at RT (25°C).

For the self-healing tests, the middle part of copolymer films was cut by razor blade, reattached within 1 min, and healed for 24 hours at RT, unless specified. The tensile stress-stretch measurements were performed for the healed copolymer films, under the same condition with undamaged specimens. The self-healing efficiency  $\eta_{\text{heal}}$  was defined as the stretch energy density (under area of stress-stretch curves) ratio of healed ( $U_{\text{heal}}$ ) to undamaged ( $U_0$ ) specimens (Fig. 2A).

The tensile loading-unloading of copolymer films were conducted with the universal testing machine, with varying applied stretch  $\lambda_{\text{app}}$ . The stretch rate was 2 min<sup>-1</sup>. Fracture test specimens were prepared by half-notched in the middle point of the specimens, and fracture energy  $\Gamma$  is defined as the work done by unnotched sample until the critical distance  $d_c$  of notched sample,  $U(d_c)$ , divided by the width  $w_0$  and the thickness  $t_0$  of the unnotched sample. The stretch rate was 5 min<sup>-1</sup>.

### Differential scanning calorimetry measurement

To define the glass transition temperature ( $T_g$ ) of the copolymer films, the differential scanning calorimetry (DSC) experiments (Discovery DSC, TA Instruments) were conducted. The sample of 5 to 10 mg was placed in a nonhermetic pan, and an empty pan was used as a reference. All of the samples were heated from -80° to 80°C with 10°C min<sup>-1</sup>, wherein the thermal transitions for the heating cycle were recorded. The  $T_g$  was determined by the inflection point of the heat capacity in the cycle. The  $T_g$  of homopolymer was also measured with the same measurement procedure. Note that poly(2-ethylhexyl acrylate) did not show clear inflection point in the lower limit temperature of the instrument (-80°C); we cited its  $T_g$  value (-80°C) reported in the literature (41).

### MD simulations

MD simulations were conducted using COMPASS II force field equipped in Forcite module in Materials Studio software (BIOVIA Inc.). The atactic copolymers with thirty monomers were generated according to the monomer combination and composition. The 20 chains of copolymers were randomly packed in a box at an initial density of 0.7 g cm<sup>-3</sup>. The generated model system was geometrically optimized and equilibrated through MD simulation with NPT ensemble (i.e., isobaric-isothermal) at 298 K and 1 atm for 300 ps using Nose thermostat and Berendsen barostat. For the production step, MD simulation was conducted for 100 ps using NPT ensemble. The time step for all MD simulation set to 1 fs. The interaction energy is calculated by difference between the energy of total system and the

sum of energies of separated polymer chain systems. The MSD have been calculated on the basis of Eq. 1

$$\text{MSD} = \frac{1}{N_{\text{bb}}} \sum_{i=1}^{N_{\text{bb}}} |x_i(t) - x_i(0)|^2 \quad (1)$$

where  $N_{\text{bb}}$  is a number of total chain and  $x_i(t)$  is the center of mass of backbone atom of  $i$ th polymer chain and end group at time  $t$ . RDF,  $g(r)$ , has been calculated on the basis of Eq. 2

$$g(r) = \frac{1}{\rho 4\pi r^2} \frac{\sum_{t=1}^K \sum_{i=1}^N \Delta N_i(r \rightarrow r + \delta_r)}{NK} \quad (2)$$

where  $\rho$  is the number density,  $K$  is the number of time step,  $N$  is the total number of atom, and  $\Delta N_i$  is the number of considered particle between  $r$  and  $r + \delta_r$ . The simulation was independently conducted three times with different conformation (fig. S22). Unless otherwise stated, the simulations were conducted with aforementioned conditions.

### Calculation of the $T_g$ of random copolymers by MD simulation

To calculate the  $T_g$  of the random copolymer series, 20 chains of random copolymer were randomly arranged, and then the geometry was optimized and equilibrated at a sufficient high temperature and 1 atm using the NPT ensemble for 200 ps. The equilibrated temperature is varied according to the species. The equilibrated structure was cooled down with the temperature interval of 15 K for 150 ps. The MSD of last 50 ps was averaged and reported as a MSD at each temperature. The MSD was plotted according to the temperature and linear-fitted into two lines grouping the points with similar slope. The  $T_g$  of copolymer was calculated as the temperature of the cross-point of two fitted line (fig. S25).

### Microcrack MD simulations

Initially, the 40 chains of tBu-Eh-0.8 random copolymers were equilibrated at 298 K and 1 atm for 200 ps. The length of the simulation box along  $x$  axis was elongated to 200 Å and equilibrated under 298 K for 100 ps. The microcracks were generated by splitting the polymer chains in half (i.e., 20 each) along the  $x$  axis and separating them by crack size,  $L$ —15, 7, and 2 Å. Each of five carbon atoms of different polymers located on the leftmost and rightmost surfaces was fixed. The polymer chains that interact with those at the opposite side of crack were defined as interfacial chains. After geometrically optimization step, the simulation was conducted under constant temperature of 298 K using the NVT ensemble (i.e., isochoric-isothermal) for 400 ps. The pristine state was obtained by conducting simulation under same condition without initial crack to obtain sufficiently randomized structure. The interaction energy of the system was defined as a nonbonded interatomic interaction of van der Waals and electrostatic interaction and calculated according to the simulation time. The first peak value of RDF between tBu-tBu was calculated to investigate the extent of chain diffusion and randomization of polymer chains. The obtained properties of the pristine state are the average of the last 100 ps of the simulation.

### Dielectric spectra measurement

To measure the polarity of copolymers, dielectric constant measurement was performed using LCR meter (E4980A precision LCR meter, Agilent Technologies), equipped with accessories of dielectric test

fixture and software (16451B and N1500A). The specimens were located within two parallel metal plates of the fixtures and gently contacted. Dielectric constant  $\epsilon_r$  and dielectric loss  $\epsilon''/\epsilon'$  of the copolymers were obtained by frequency sweeps from 200 Hz to 1 MHz at RT.

### Hydrophobicity measurement

To verify the hydrophobicity of the copolymers, the contact angle between 5- $\mu$ l droplet of deionized water and the specimen was measured using a contact angle analyzer (FEMTOFAB, Smart Drop) at RT. To verify water effect on mechanical and self-healing properties of the copolymers, the samples were firstly immersed in water or saline (3.5 wt % of sodium chloride solution and artificial seawater). After 30 min, the middle point of specimens was cut, attached within 1 min, and then healed in water or saline for 24 hours at RT. Then, the samples underwent tensile stress-stretch measurements.

### Transmittance measurement

Transmittance of the copolymer films (thickness of 400  $\mu$ m) in the range of 300 to 800 nm was obtained by a UV-visible spectrometer (Cary 60 UV-Vis, Agilent Technologies).

### Rheological properties measurement

Tensile stress relaxation tests were performed by the universal testing machine. The specimens with 30 mm by 10 mm by 0.4 mm (width  $\times$  length  $\times$  thickness; 5 mm of gauge length) were mounted on clamps and subjected to stretch two times of its original length during 1 min. Then, the specimens were hold at the stretch for 80,000 s. The obtained stress-time curves were fitted to Zener model, where the obtained parameters are shown in fig. S30. For the comparison, commercial Bu rubbers (pieces of Bu gloves, IN-G800B, iNexus Inc.) were subjected to same stress relaxation tests.

The viscoelastic response of the copolymers was determined by using DHR-2 (TA Instruments). Rheological frequency sweeps, from 0.1 to 100  $\text{rad s}^{-1}$  with 0.1% applied shear strain in parallel plate geometry, were performed over a wide range of temperature from 0° to 125°C. The copolymer samples were cut to disc-shape specimens with a thickness of  $\sim$ 400  $\mu$ m and a diameter of 20 mm.

### Supplementary Materials

#### This PDF file includes:

Supplementary Text  
Figs. S1 to S35  
Table S1  
Legends for movies S1 to S3  
References

#### Other Supplementary Material for this manuscript includes the following:

Movies S1 to S3

### REFERENCES AND NOTES

1. M. Hager, P. Greil, C. Leyens, S. van der Zwaag, U. S. Schubert, Self-healing materials. *Adv. Mater.* **22**, 5424–5430 (2010).
2. J. F. Patrick, M. J. Robb, N. R. Sottos, J. S. Moore, S. R. White, Polymers with autonomous life-cycle control. *Nature* **540**, 363–370 (2016).
3. R. P. Wool, K. M. O'Connor, A theory crack healing in polymers. *J. Appl. Phys.* **52**, 5953–5963 (1981).
4. R. P. Wool, Self-healing materials: A review. *Soft Matter* **4**, 400–418 (2008).
5. S. Wang, M. W. Urban, Self-healing polymers. *Nat. Rev. Mater.* **5**, 562–583 (2020).



6. R. P. Sijbesma, F. H. Beijer, L. Brunsveld, B. J. B. Folmer, J. H. K. K. Hirschberg, R. F. M. Lange, J. K. L. Lowe, E. W. Meijer, Reversible polymers formed from self-complementary monomers using quadruple hydrogen bonding. *Science* **278**, 1601–1604 (1997).
7. P. Cordier, F. Tournilhac, C. Soulié-Ziakovic, L. Leibler, Self-healing and thermoreversible rubber from supramolecular assembly. *Nature* **451**, 977–980 (2008).
8. Y. Yanagisawa, Y. Nan, K. Okuro, T. Aida, Mechanically robust, readily repairable polymers via tailored noncovalent cross-linking. *Science* **359**, 72–76 (2018).
9. J. Wu, L. H. Cai, D. A. Weitz, Tough self-healing elastomers by molecular enforced integration of covalent and reversible networks. *Adv. Mater.* **29**, 1–8 (2017).
10. Q. Wang, J. L. Mynar, M. Yoshida, E. Lee, M. Lee, K. Okuro, K. Kinbara, T. Aida, High-water-content mouldable hydrogels by mixing clay and a dendritic molecular binder. *Nature* **463**, 339–343 (2010).
11. A. Phadke, C. Zhang, B. Arman, C. C. Hsu, R. A. Mashelkar, A. K. Lele, M. J. Tauber, G. Arya, S. Varghese, Rapid self-healing hydrogels. *Proc. Natl. Acad. Sci. U.S.A.* **109**, 4383–4388 (2012).
12. J. Kang, D. Son, G. J. N. Wang, Y. Liu, J. Lopez, Y. Kim, J. Y. Oh, T. Katsumata, J. Mun, Y. Lee, L. Jin, J. B. H. Tok, Z. Bao, Tough and water-insensitive self-healing elastomer for robust electronic skin. *Adv. Mater.* **30**, e1706846 (2018).
13. A. Harada, R. Kobayashi, Y. Takashima, A. Hashidzume, H. Yamaguchi, Macroscopic self-assembly through molecular recognition. *Nat. Chem.* **3**, 34–37 (2011).
14. S. Nomimura, M. Osaki, J. Park, R. Ikura, Y. Takashima, H. Yamaguchi, A. Harada, Self-healing alkyl acrylate-based supramolecular elastomers cross-linked via host-guest interactions. *Macromolecules* **52**, 2659–2668 (2019).
15. M. Burnworth, L. Tang, J. R. Kumpfer, A. J. Duncan, F. L. Beyer, G. L. Fiore, S. J. Rowan, C. Weder, Optically healable supramolecular polymers. *Nature* **472**, 334–337 (2011).
16. H. Ceylan, M. Urel, T. S. Erkal, A. B. Tekinay, A. Dana, M. O. Guler, Mussel inspired dynamic cross-linking of self-healing peptide nanofiber network. *Adv. Funct. Mater.* **23**, 2081–2090 (2013).
17. C. H. Li, C. Wang, C. Keplinger, J. L. Zuo, L. Jin, Y. Sun, P. Zheng, Y. Cao, F. Lissel, C. Linder, X. Z. You, Z. Bao, A highly stretchable autonomous self-healing elastomer. *Nat. Chem.* **8**, 618–624 (2016).
18. Y. L. Rao, A. Chortos, R. Pfattner, F. Lissel, Y. C. Chiu, V. Feig, J. Xu, T. Kurosawa, X. Gu, C. Wang, M. He, J. W. Chung, Z. Bao, Stretchable self-healing polymeric dielectrics cross-linked through metal-ligand coordination. *J. Am. Chem. Soc.* **138**, 6020–6027 (2016).
19. A. Das, A. Sallat, F. Böhme, M. Suckow, D. Basu, S. Wießner, K. W. Stöckelhuber, B. Voit, G. Heinrich, Ionic modification turns commercial rubber into a self-healing material. *ACS Appl. Mater. Interfaces* **7**, 20623–20630 (2015).
20. T. L. Sun, T. Kurokawa, S. Kuroda, A. Bin Ihsan, T. Akasaki, K. Sato, M. A. Haque, T. Nakajima, J. P. Gong, Physical hydrogels composed of polyampholytes demonstrate high toughness and viscoelasticity. *Nat. Mater.* **12**, 932–937 (2013).
21. Y. Peng, L. Zhao, C. Yang, Y. Yang, C. Song, Q. Wu, G. Huang, J. Wu, Super tough and strong self-healing elastomers based on polyampholytes. *J. Mater. Chem. A* **6**, 19066–19074 (2018).
22. X. Qu, W. Niu, R. Wang, Z. Li, Y. Guo, X. Liu, J. Sun, Solid-state and liquid-free elastomeric ionic conductors with autonomous self-healing ability. *Mater. Horizons* **7**, 2994–3004 (2020).
23. D. C. Tuncaboylu, M. Sari, W. Oppermann, O. Okay, Tough and self-healing hydrogels formed via hydrophobic interactions. *Macromolecules* **44**, 4997–5005 (2011).
24. Y. Cao, T. G. Morrissey, E. Acome, S. I. Allec, B. M. Wong, C. Keplinger, C. Wang, A. Transparent, Self-healing, highly stretchable ionic conductor. *Adv. Mater.* **29**, 1–9 (2017).
25. X. Ming, J. Du, C. Zhang, M. Zhou, G. Cheng, H. Zhu, Q. Zhang, S. Zhu, All-solid-state self-healing ionic conductors enabled by ion-dipole interactions within fluorinated poly(ionic liquid) copolymers. *ACS Appl. Mater. Interfaces* **13**, 41140–41148 (2021).
26. S. Burattini, B. W. Greenland, D. H. Merino, W. Weng, J. Seppala, H. M. Colquhoun, W. Hayes, M. E. MacKay, I. W. Hamley, S. J. Rowan, A healable supramolecular polymer blend based on aromatic  $\pi$ - $\pi$  stacking and hydrogen-bonding interactions. *J. Am. Chem. Soc.* **132**, 12051–12058 (2010).
27. J. F. Mei, X. Y. Jia, J. C. Lai, Y. Sun, C. H. Li, J. H. Wu, Y. Cao, X. Z. You, Z. Bao, A highly stretchable and autonomous self-healing polymer based on combination of Pt–Pt and  $\pi$ - $\pi$  interactions. *Macromol. Rapid Commun.* **37**, 1667–1675 (2016).
28. M. W. Urban, D. Davydovich, Y. Yang, T. Demir, Y. Zhang, L. Casabianca, Key-and-lock commodity self-healing copolymers. *Science* **362**, 220–225 (2018).
29. S. Wang, M. W. Urban, Self-healable fluorinated copolymers governed by dipolar interactions. *Adv. Sci.* **8**, 1–7 (2021).
30. Y. Liu, T. Chen, Z. Jin, M. Li, D. Zhang, L. Duan, Z. Zhao, C. Wang, Tough, stable and self-healing luminescent perovskite-polymer matrix applicable to all harsh aquatic environments. *Nat. Commun.* **13**, 1–11 (2022).
31. X. Chen, M. A. Dam, K. Ono, A. Mal, H. Shen, S. R. Nutt, K. Sheran, F. Wudl, A thermally re-mendable cross-linked polymeric material. *Science* **295**, 1698–1702 (2002).
32. Y. Amamoto, J. Kamada, H. Otsuka, A. Takahara, K. Matyjaszewski, Repeatable photoinduced self-healing of covalently cross-linked polymers through reshuffling of trithiocarbonate units. *Angew. Chem. Int. Ed.* **50**, 1660–1663 (2011).
33. J. J. Cash, T. Kubo, A. P. Bapat, B. S. Sumerlin, Room-temperature self-healing polymers based on dynamic-covalent boronic esters. *Macromolecules* **48**, 2098–2106 (2015).
34. Y. Chen, A. M. Kushner, G. A. Williams, Z. Guan, Multiphase design of autonomic self-healing thermoplastic elastomers. *Nat. Chem.* **4**, 467–472 (2012).
35. H. Wang, Y. Yang, M. Nishiura, Y. Higaki, A. Takahara, Z. Hou, Synthesis of self-healing polymers by scandium-catalyzed copolymerization of ethylene and anisylpropylenes. *J. Am. Chem. Soc.* **141**, 3249–3257 (2019).
36. C. C. Huang, M. X. Du, B. Q. Zhang, C. Y. Liu, Glass Transition Temperatures of Copolymers: Molecular Origins of Deviation from the Linear Relation. *Macromolecules* **55**, 3189–3200 (2022).
37. S. Gaikwad, M. W. Urban, Ring-and-lock interactions in self-healable styrenic copolymers. *J. Am. Chem. Soc.* **145**, 9693–9699 (2023).
38. M. Rubinstein, R. H. Colby, *Polymer Physics* (Oxford Univ. Press, 2003).
39. M. Li, L. Chen, Y. Li, X. Dai, Z. Jin, Y. Zhang, W. Feng, L. T. Yan, Y. Cao, C. Wang, Superstretchable, yet stiff, fatigue-resistant ligament-like elastomers. *Nat. Commun.* **13**, 1–8 (2022).
40. G. J. Lake, Fatigue and fracture of elastomers. *Rubber Chem. Technol.* **68**, 435–460 (1995).
41. L. A. Cannon, R. A. Pethrick, Effect of the glass-transition temperature on film formation in 2-ethylhexyl acrylate/methyl methacrylate emulsion copolymers. *Macromolecules* **32**, 7617–7629 (1999).
42. M. Gordon, J. S. Taylor, Ideal copolymers and the second-order transitions of synthetic rubbers. i. Non-crystalline copolymers. *J. Appl. Chem.* **2**, 493–500 (1952).
43. F. Tanaka, S. F. Edwards, Viscoelastic properties of physically crosslinked networks. *J. Nonnewton. Fluid Mech.* **43**, 273–288 (1992).
44. C. Tang, Y. Tang, Y. Ye, Z. Yan, Z. Chen, L. Chen, L. Zhang, J. Liu, J. Shi, H. Xia, W. Hong, Identifying the conformational isomers of single-molecule cyclohexane at room temperature. *Chem* **6**, 2770–2781 (2020).
45. D. M. Davies, Hysteresis in rubber. *Nature* **170**, 937 (1952).

#### Acknowledgments

**Funding:** This work was supported by the LG Display (C2022007501). This work was supported by the Pioneer Research Center Program through the National Research Foundation of Korea (NRF) funded by the Ministry of Science, ICT & Future Planning (grant no. NRF-2022M3C1A3081211). This work was supported by NRF grants funded by the Korean Government (2018M3A7B4089670, 2021R1A2C2092737, and RS-2023-00257666). **Author contributions:** Conceptualization and supervision: J.-Y.S., J.-M.P., and S.K.K. Methodology: J.-Y.S. and J.-M.P. Resources, funding acquisition, and data curation: J.-Y.S. and S.K.K. Project administration: J.-Y.S., C.S.P., and S.K.K. Investigation: C.S.P., J.-M.P., and S.K.K. Formal analysis: C.S.P. and J.-M.P. All authors validated and visualized the results and wrote the manuscript. **Competing interests:** The authors declare that they have no competing interests. **Data and materials availability:** All data needed to evaluate the conclusions in the paper are present in the paper and/or the Supplementary Materials.

Submitted 5 March 2024

Accepted 5 June 2024

Published 10 July 2024

10.1126/sciadv.adp0729